Coal fly ash is a major carbon flux in the Chang Jiang (Yangtze River) basin

Gen K. Li[a,b,1], Woodward W. Fischer[b], Michael P. Lamb[b], A. Joshua West[c], Ting Zhang[a], Valier Galy[d], Xingchen Tony Wang[b,e], Shilei Li (李石磊)[a], Hongrui Qiu[f], Gaojun Li[a], Liang Zhao[a], Jun Chen[a], and Junfeng Ji[a]

[a]Key Laboratory of Surficial Geochemistry, Ministry of Education, School of Earth Sciences and Engineering, Nanjing University, Nanjing 210023, China; [b]Division of Geological and Planetary Sciences, California Institute of Technology, Pasadena, CA 91125; [c]Department of Earth Sciences, University of Southern California, Los Angeles, CA 90089; [d]Department of Marine Chemistry and Geochemistry, Woods Hole Oceanographic Institute, Woods Hole, MA 02543; [e]Department of Earth and Environmental Sciences, Boston College, Chestnut Hill, MA 02467; and [f]Department of Earth, Environmental and Planetary Sciences, Rice University, Houston, TX 77005

Edited by Donald E. Canfield, University of Southern Denmark, Odense M., Denmark, and approved March 25, 2021 (received for review December 9, 2019)

Fly ash—the residuum of coal burning—contains a considerable amount of fossilized particulate organic carbon (FOC_{ash}) that remains after high-temperature combustion. Fly ash leaks into natural environments and participates in the contemporary carbon cycle, but its reactivity and flux remained poorly understood. We characterized FOC_{ash} in the Chang Jiang (Yangtze River) basin, China, and quantified the riverine FOC_{ash} fluxes. Using Raman spectral analysis, ramped pyrolysis oxidation, and chemical oxidation, we found that FOC_{ash} is highly recalcitrant and unreactive, whereas shale-derived FOC (FOC_{rock}) was much more labile and easily oxidized. By combining mass balance calculations and other estimates of fly ash input to rivers, we estimated that the flux of FOC_{ash} carried by the Chang Jiang was 0.21 to 0.42 Mt C·y^{-1} in 2007 to 2008—an amount equivalent to 37 to 72% of the total riverine FOC export. We attributed such high flux to the combination of increasing coal combustion that enhances FOC_{ash} production and the massive construction of dams in the basin that reduces the flux of FOC_{rock} eroded from upstream mountainous areas. Using global ash data, a first-order estimate suggests that FOC_{ash} makes up to 16% of the present-day global riverine FOC flux to the oceans. This reflects a substantial impact of anthropogenic activities on the fluxes and burial of fossil organic carbon that has been made less reactive than the rocks from which it was derived.

coal | fly ash | carbon cycle | Chang Jiang (Yangtze River) | sediment transport

Fossil particulate organic carbon (FOC) is a geologically stable form of carbon that was produced by the ancient biosphere and then buried and stored in the lithosphere; it is a key player in the geological carbon cycle (1–7). Uplift and erosion liberate FOC from bedrock, delivering it to the surficial carbon cycle. Some is oxidized in sediment routing systems, but a portion escapes and can be transported by rivers to the oceans (5, 8–10). Oxidation of FOC represents a long-term atmospheric carbon source and O_2 sink, whereas the reburial of FOC in sedimentary basins has no long-term net effect on atmospheric CO_2 and O_2 (1, 9, 11). Exhumation and erosion of bedrock provide a natural source of FOC (2, 8), which we refer to as FOC_{rock}. Human activities have introduced another form of FOC from the mining and combustion of coal. Burning coal emits CO_2 to the atmosphere but also leaves behind solid waste that contains substantial amounts of organic carbon (OC) that survives high-temperature combustion (12–14). This fossil-fuel-sourced carbon represents a poorly understood anthropogenic flux in the global carbon cycle; it also provides a major source of black carbon, which is a severe pollutant and climate-forcing agent (12–15).

Previous studies sought to quantify black carbon in different terrestrial and marine environments and to distinguish fossil fuel versus forest fire sources (14–18). In this study, we focused on fly ash—the material left from incomplete coal combustion. As a major fossil fuel, coal supplies around 30% of global primary energy consumption (19, 20). Despite efforts to capture and utilize fly ash, a fraction enters soils and rivers; the resulting fossil OC from fly ash (FOC_{ash}) has become a measurable part of the contemporary carbon cycle (14). FOC_{ash} is also referred to as "unburned carbon" in fly ash (21–25); it provides a useful measure of combustion efficiency and the quality of fly ash as a building material (e.g., in concrete) (23–26). Industrial standards of FOC_{ash} content in fly ash have been established for material quality assurance (23, 24, 26, 27). However, the characteristics and fluxes of FOC_{ash} released to the environment, and how these compare to FOC_{rock} from bedrock erosion, remain less well understood.

To fill this knowledge gap, we examined the Chang Jiang (Yangtze River) basin in China—a system that allowed us to evaluate the influence of FOC_{ash} on the carbon cycle at continental scales. In the 2000s, China became the largest coal-consuming country in the world, with an annual coal consumption of over 2,500 Mt, equating to ∼50% of worldwide consumption (19, 20, 28). Coal contributed over 60% of China's national primary energy consumption through the 2000s. A significant portion of this coal (approximately one-third) was consumed in the Chang Jiang (CJ) basin, where China's most populated and economically developed areas are located (29). Significant amounts of fly ash and FOC_{ash} continue to be produced and consumed in the CJ basin. To determine the human-induced FOC_{ash} flux, we investigated the FOC_{ash} cycle in the CJ basin. We characterized OC in a series of samples including fly ash, bedrock sedimentary shale,

Significance

Coal combustion releases CO_2 but also leaves behind solid waste, or fly ash, which contains considerable amounts of carbon. The organic carbon sourced from fly ash resists chemical breakdown, and we find that it now contributes nearly half of the fossil organic carbon exported by the Chang Jiang—the largest river in Asia. The fly ash flux in this basin is similar to the natural sediment flux to the oceans because dam building has reduced sediment transport, while increased coal consumption generates abundant fly ash. Our results show that fly ash is an important component of the present-day carbon load in rivers and illustrates that human-driven carbon cycling can match the pace of the geological carbon cycle at decadal timescales.

Author contributions: G.K.L., W.W.F., M.P.L., A.J.W., J.C., and J.J. designed research; G.K.L., T.Z., X.T.W., and S.L. performed research; G.K.L., T.Z., V.G., and J.J. contributed new reagents/analytic tools; G.K.L., W.W.F., M.P.L., V.G., X.T.W., S.L., H.Q., G.L., L.Z., and J.J. analyzed data; and G.K.L., W.W.F., M.P.L., A.J.W., T.Z., V.G., X.T.W., S.L., G.L., L.Z., J.C., and J.J. wrote the paper.

The authors declare no competing interest.

This article is a PNAS Direct Submission.

[1]To whom correspondence may be addressed. Email: ligen@caltech.edu.

This article contains supporting information online at https://www.pnas.org/lookup/suppl/doi:10.1073/pnas.1921544118/-/DCSupplemental.

Published May 17, 2021.

and river sediment through multiple geochemical analyses. We then estimated the CJ-exported FOC_{ash} flux and evaluated how human activities modulated FOC transfer at basin scales. We found that in the CJ basin, coal combustion and dam construction have conspired to boost the FOC_{ash} flux and reduce the FOC_{rock} flux carried by the CJ; as a result, these two fluxes converged over an interval of 60 y.

The CJ Basin

The CJ basin is located in central China and has a drainage area of around 1,800,000 km^2—nearly 20% of the total terrestrial area of China (30, 31). Originating from the Tibetan Plateau, the CJ drains mountainous areas in its upper reach and alluvial plains in its lower reach, before emptying into the Eastern China Sea (Fig. 1). The regional climate is controlled by the East Asian monsoon with peak precipitation and associated floods occurring from May to September (30, 31). The bedrock geology of the CJ basin is mainly composed of sedimentary rocks, with minor igneous and metamorphic exposures (Fig. 1*A*) (32, 33).

Over the past 60 y, the CJ basin has undergone significant anthropogenic change including the massive construction of industrial and hydrological infrastructure (e.g., coal-fired power plants and dams) and increased coal combustion (Fig. 1 *B* and *C*) (34–36). More than 50,000 dams, including the world's largest—the Three Gorges Dam—have been built in the CJ basin; these dams trap sediment in the resulting reservoirs and have significantly reduced the CJ sediment export to the ocean (Fig. 2) (34, 37). In the process, they profoundly altered the natural transfer of carbon (38, 39). The growth in China's coal consumption over the past decades has also fundamentally altered the CJ basin, and the annual production of fly ash is, remarkably, now comparable in total mass to the entire CJ sediment flux (Fig. 2). It is not a surprise, then, that fly ash particles and associated black carbon have been observed in recent river and delta sediment in the CJ basin (16, 40–43).

Materials and Approaches

We sampled fly ash, shale, river sediment, and plant debris (leaves of typical plants) in the middle-lower CJ basin and collected samples from a core drilled

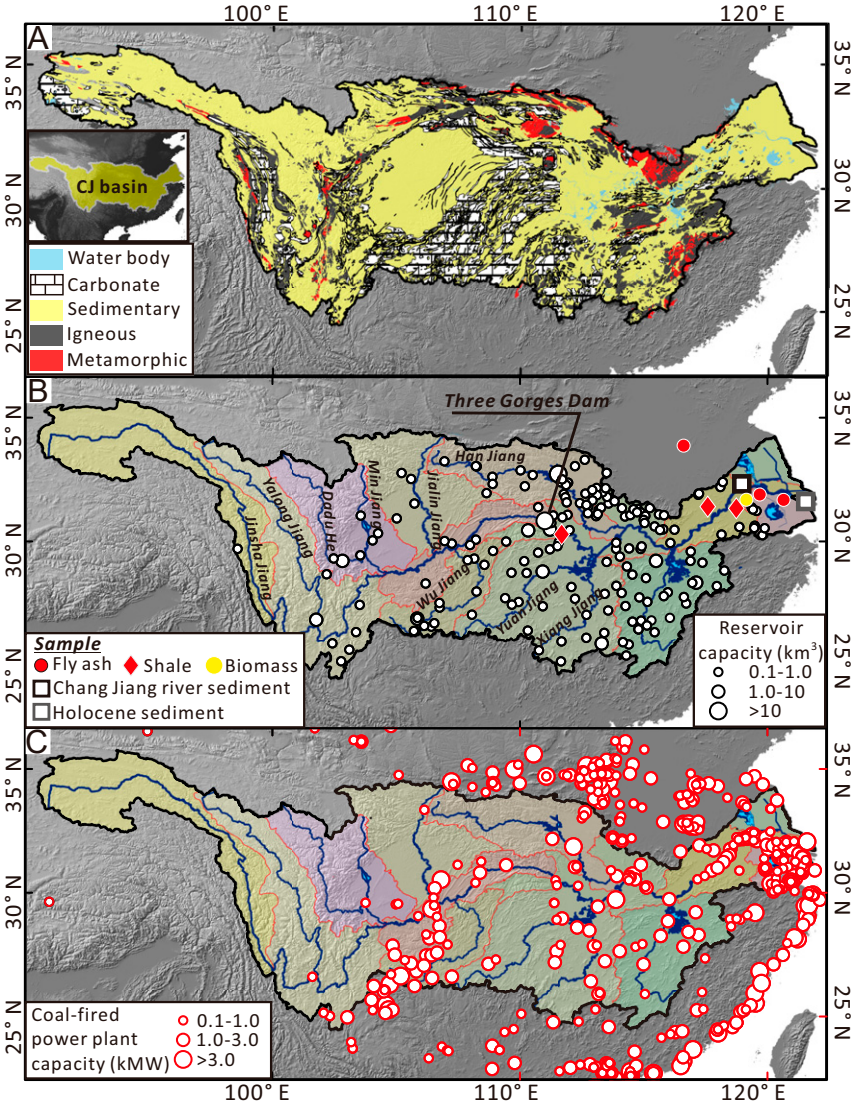

Fig. 1. Maps of the CJ (Yangtze River) basin including (*A*) bedrock geology and (*Inset*) regional context (33, 38), (*B*) the distribution of reservoirs (capacity >0.1 km^3) with the major tributaries of the CJ denoted (details in *SI Appendix*), and (*C*) the distribution of major coal-fired power plants (capacity >100 MW) (details in *SI Appendix*).

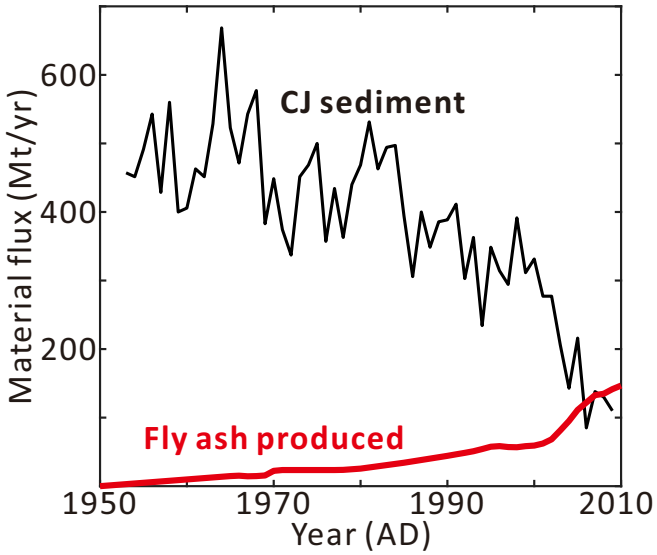

Fig. 2. Time series of annual sediment export fluxes by the CJ plotted alongside fly-ash production in the basin during 1950 to 2010 (details in *SI Appendix*).

into the CJ estuary delta recovering Holocene sediment (Fig. 1). To characterize OC in the samples, we measured OC content and conducted chemical oxidation experiments, ramped pyrolysis oxidation (RPO) analysis, and Raman spectral analysis (details in *SI Appendix*).

Characteristics of Fly-Ash-Sourced OC. The CJ fly-ash samples we have studied have an FOC_{ash} content ($[FOC]_{ash}$) of $2.25^{+1.63}/_{-1.18}$% (Fig. 3*A*, reported as the median and 16th and 84th percentiles)—a value 2 to 100 times higher than the FOC content in global river sediments (38, 44). The measured FOC_{ash} content is comparable to the Chinese industrial standard (GB/T 477-2008) of 5% for use in concrete and cement and to the standards of FOC_{ash} content in other major coal-consuming countries (*SI Appendix*, section S6) (24, 26, 27).

In general, FOC_{ash} comprises a spectrum of carbon species with different forms and origins (21–24). Substantial effort in prior work has been spent on imaging, characterizing, and separating FOC_{ash} of different carbon species (e.g., refs. 23, 24, 45–48 and *SI Appendix*, section S6). Notably, studies using electron microscopy found that FOC_{ash} includes nanometer-scale soot particles, micrometer-sized char particles, and carbon associated with inorganic minerals (23, 24, 48–50). The relative abundances of the different carbon forms in fly ash vary due a range of factors including coal rank and combustion conditions (22, 23, 51, 52), as well as separation method (see more discussion in *SI Appendix*, section S7). A study using liquid-suspension gravity separation found that soot represents a nonnegligible component in fly ash, contributing ~35% carbon mass to the total FOC_{ash} (53).

Raman spectral analyses of our CJ samples provided insight into the chemical moieties of FOC_{ash}, specifically the presence of graphitic structure and its association with minerals (Fig. 3*B* and *SI Appendix*, Figs. S2 and S3). Graphitic carbon was indicated by characteristic G and D bands, at ~1,350 cm^{-1} and ~1,600 cm^{-1}, respectively (Fig. 3*B* and *SI Appendix*, Figs. S2 and S3), with the G band corresponding to graphite and the D band induced by defects (5, 54). Nongraphitic carbon, or carbon bonded to heteroatoms (e.g., nitrogen and oxygen), likely caused the high background florescence observed in some samples (*SI Appendix*, Fig. S2) (55). Mineral-associated carbon featured spectral peaks of minerals and graphitic carbon, and often high background fluorescence (Fig. 3*B* and *SI Appendix*, Fig. S2). The Raman analyses also resolved FOC_{ash} as individual carbon particles, displaying no close association with minerals (Fig. 3*B* and *SI Appendix*, Figs. S2 and S3)—textures consistent with other observations of char and soot particles in coal ash (23, 24). We collected a total of 30 Raman spectra in seven of the CJ ash samples: 20 of these displayed mineral-associated carbon containing both graphitic and nongraphitic carbon, 5 revealed graphitic carbon not associated with minerals, and the remaining 5 displayed mixtures of graphitic and nongraphitic carbon not in association with minerals (*SI Appendix*, Figs. S2 and S3).

Complementing the Raman data, we collected new RPO and chemical oxidation data, which showed that FOC_{ash} is much more recalcitrant than shale-derived FOC_{rock} (Fig. 3 *C* and *D*). The RPO results were reported as thermograms and translated to spectra of activation energies (E_a) (56). In the thermograms, FOC_{ash} has a higher fraction of carbon decomposed and more CO_2 released at high temperatures (e.g., >700 °C) than FOC_{rock} (*SI Appendix*, Fig. S6). Converting the thermograms to the spectra of activation energies, we found that fly ash featured much higher E_a than the shale (Fig. 3*C*) and other FOC_{rock}-dominated river sediment samples (9, 56), revealing a high thermal stability and an extremely refractory phase of FOC_{ash} (E_a >220 kJ/mol). The chemical oxidation experiments employed sodium persulfate ($Na_2S_2O_8$)—a chemical with a very high oxidation potential (standard oxidation–reduction potential is E^0 ~2.01V) comparable to O_3 (E^0 ~2.07V) and much higher than O_2 (E^0 ~1.23V) (57). This agent has been used in soil studies to simulate oxidation in natural environments (58). The results from oxidation experiments are reported as f_{ox}, the mass fraction of OC that gets oxidized in the experiments. A low f_{ox} value means the sample was difficult to oxidize and contains a high proportion of OC that is recalcitrant. For the fly ash samples, f_{ox} is low (0 to 0.25), as expected since FOC_{ash} has undergone pedogenesis, petrogenesis, and high-temperature incineration, leaving behind the most refractory OC class (14). For shale samples, f_{ox} values were much higher (0.4 to 0.85), implying that a significant portion of FOC_{rock} is reactive and labile, which is consistent with field observations of substantial loss of FOC_{rock} in soils and sediment routing systems (5, 59, 60). Expectedly, the plant samples were highly labile, with a high f_{ox} of 0.9 to 1.

Although current methods cannot delineate the microscale (nanometer to micrometer) characteristics of FOC_{ash} and directly quantify all the different carbon forms in fly ash (*SI Appendix*, section S2), our Raman and RPO results together provided constraints on the carbon species composing FOC_{ash} in our samples—and this compositional information helped explain results from the oxidation experiments. First, the Raman data indicated the presence of multiple different carbon species, including the dominance of mineral-associated carbon. Second, considering that graphitic carbon is thermally decomposed at temperatures of 700 to 800 °C, the RPO thermograms designated that 20 to 50% of FOC_{ash} is composed of graphitic carbon (*SI Appendix*, Fig. S4) (61). Altogether, these analyses of our fly ash samples reveal that graphitic carbon is the major constituent in FOC_{ash} and nongraphitic carbon occurs mostly in association with minerals. These two forms of carbon—graphitic and mineral-associated—hinted at two plausible mechanisms for preserving FOC_{ash} during high-temperature combustion: selective preservation as stable graphitic carbon and mineral protection (62, 63). Nongraphitic carbon is less recalcitrant than graphitic carbon (5, 47). Thus, the relative proportions of graphitic versus nongraphitic carbon may also explain the natural variation in f_{ox} observed in our fly ash samples (Fig. 3 and *SI Appendix*, Figs. S2 and S3). In any case, the low f_{ox} of FOC_{ash} underscored its recalcitrance; simply put, it is a less reactive component in the surficial carbon cycle than rock-derived FOC.

OC in the CJ River Sediments. Chemical oxidation procedures, in conjunction with radiocarbon analyses, also helped resolve the bulk composition of riverine OC. OC in river sediment represents a mixture of radiocarbon-enriched biospheric OC and radiocarbon-dead FOC (11, 64). In f_{ox}-1/OC space, CJ suspended sediment sits on a mixing trend between a biospheric OC end member and a radiocarbon-dead FOC end member (Fig. 3*D* and *SI Appendix*). Coupling this mixing relationship with prior chemical oxidation results reveals that CJ river FOC could not be oxidized via the chemical treatment method and made up 85% of the residual OC after oxidation (38).

The f_{ox} of the core sediment samples from the CJ estuary had a range similar to the CJ suspended sediment samples (0.5 to 0.8). Those samples came from floodplain and fluvial sedimentary facies (65), representing ash-uncontaminated, preindustrial CJ sediment. If we assumed a behavior of FOC in those preindustrial samples similar to that found during the oxidation experiment (i.e., riverine FOC cannot be oxidized and makes up 85% of the residual OC after oxidation), we estimated a $FOC_{preindustrial}$ content of 0.15 ± 0.02%—a value 6 to 30 times lower than $[FOC]_{ash}$ ($2.25^{+1.63}/_{-1.18}$%). We treated this estimate as an approximation of rock-derived FOC in the modern CJ sediment (FOC_{CJ0}) without FOC_{ash} contamination. Note that FOC_{CJ0} represents the final product of FOC_{rock} after alteration during erosion and transfer before entering the sedimentary OC pool, thus it is not necessarily equivalent to the fresh FOC_{rock} derived from rocks within the CJ basin. To validate our estimate of $[FOC]_{preindustrial}$, we defined a similar OC mixing trend for preindustrial CJ sediment using our inferred FOC end member (f_{ox} = 0 and [FOC] = 0.15 ± 0.02%) and the biospheric OC end member (Fig. 3*D*). The Holocene sediment samples fit this mixing trend (Fig. 3*D*), suggesting our estimate of $[FOC]_{preindustrial}$ is robust.

Examining the geochemical data, we also identified hydrologic and sediment transport controls on the degree of mixing observed between FOC_{ash} and FOC_{CJ0}. When separating the CJ sediment samples by river discharge (flood versus dry season) (38), distinct trends emerged (Fig. 3*E* and *SI Appendix*, Fig.

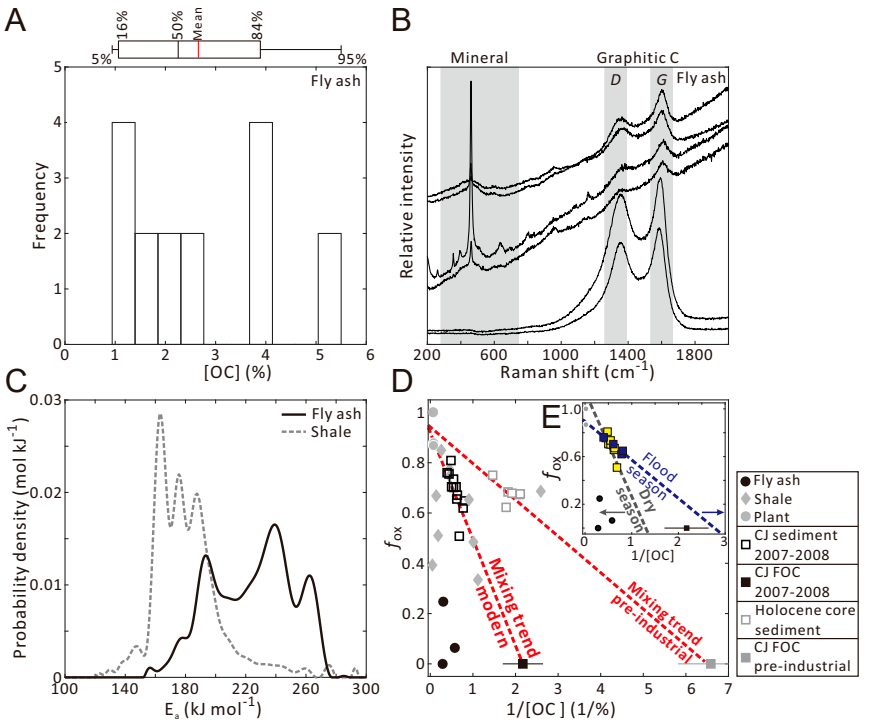

Fig. 3. Geochemical characteristics of CJ sediment and fly-ash samples. (*A*) Histograms of OC content in CJ fly-ash samples with a box-and-whisker plot showing the 5th, 16th, 50th, 84th, and 95th percentiles and mean of OC content for fly-ash samples. (*B*) Selected Raman spectra of CJ fly-ash samples showing a mix of organic and inorganic mineral phases with mineral and graphitic carbon peaks (D and G bands) denoted (for more data see *SI Appendix*, Figs. S2 and S3). (*C*) Probability density of activation energy (E_a) of a fly-ash sample and a shale sample derived from RPO results, indicating a higher modal E_a of the fly ash sample than the shale sample. (*D*) Oxidation fraction f_{ox} versus 1/[OC] (reciprocal of OC content) for studied samples, with two dashed lines indicating mixing trends between the fossil OC and biospheric OC end members. (*E*) Mixing relationships for the CJ sediment collected in the dry season (yellow) versus in the flood season (blue), defined by least-squares linear regression.

S2): The dry season featured an FOC-enriched end member, whereas the flood season marked an FOC-diluted end member. The difference could be explained by sediment transport conditions varying with the hydrograph. Fly ash is mainly composed of fine cenosphere particles (~1s to 10s μm) with a density close to or lower than typical river sediment (25, 28) and can be easily entrained by rivers during low flow. The proportion of fly ash in sediment, therefore, is lower in the flood season than in the dry season, because flooding can entrain coarser and denser sediment. The high fraction of coarse sediment and its low $[FOC]_{CJ0}$ (assuming it is equivalent to the preindustrial [FOC]) would lead to a mixed [FOC] during flooding that is lower than the dry season. Thus, our observation indicated some hydraulic control on the composition of riverine FOC as a mixture of high-[FOC] fly ash and low-[FOC] natural sediment, corroborating the low $[FOC]_{CJ0}$ seen in Holocene sediment.

Fly-Ash-Sourced OC Flux. During 2007 to 2008, around 130 Mt of fly ash was produced in the CJ basin (36% of the total fly-ash production in China; *SI Appendix*). Taking an ash utilization rate of 67% estimated for China (28), ~40 Mt of fly ash was released to the environment in the CJ basin; this is a remarkable flux given that the total CJ sediment flux is around 130 Mt·y^{-1}. There is currently no systematic storage or treatment of the unutilized ash, suggesting much of this may be released into the environment. From the budget of production alone, it is unclear how much of the wasted fly ash and FOC_{ash} enter rivers, but we can use three lines of evidence to constrain the riverine-transported FOC_{ash} flux.

First, we conducted mass balance calculations using the preindustrial [FOC] (0.15 ± 0.02%) as an approximation of the [FOC] of ash-free sediment. Assuming the modern-day CJ sediment is a mixture of fly ash and ash-uncontaminated sediment, we calculated the flux of FOC_{ash}:

$$[FOC]_{ash} \times (f_{sed-ash}) + [FOC]_{CJ0} \times (1 - f_{sed-ash}) = [FOC]_{CJ}, \quad [1]$$

where $f_{sed\text{-}ash}$ is the mass fraction of fly ash in the ash-contaminated CJ sediment and $[FOC]_{CJ}$ represents the modern-day CJ FOC. We took $2.25^{+1.63}/_{-1.18}$% for $[FOC]_{ash}$, 0.15 ± 0.02% for $[FOC]_{CJ0}$, and 0.45 ± 0.10% for $[FOC]_{CJ}$ (38), to resolve $f_{sed\text{-}ash}$ and the fraction of FOC_{ash} in the CJ-exported FOC, $f_{FOC\text{-}ash}$. We then employed Monte Carlo random sampling techniques to propagate errors and estimate uncertainties (*SI Appendix*), reported as medians and the 16th to 84th percentiles of the sampling results. We obtained a $f_{FOC\text{-}ash}$ of $72^{+8}/_{-12}$%, with a FOC_{ash} riverine flux of $0.42^{+0.14}/_{-0.15}$ Mt C, whereas the total CJ-exported FOC flux is 0.58 ± 0.13 Mt C·y^{-1} (38). We also estimated a $f_{sed\text{-}ash}$ of $13^{+18}/_{-7}$%, which is $13^{+18}/_{-7}$% of the total produced fly ash and $39^{+54}/_{-21}$% of the ash wasted in the basin (Fig. 4*A*).

Second, we referred to a prior study that estimated a $f_{sed\text{-}ash}$ of 7% based on the changes in the magnetic susceptibility (MS) of river sediment and islet deposits. An abrupt increase in the MS of the CJ sediment has been observed in recent years and attributed to the input of fly ash, which has MS ~30 times higher than ash-free sediment (40). Using a $f_{sed\text{-}ash}$ of 7%, a CJ sediment flux of 130 Mt (66), and an FOC content of $2.25^{+1.63}/_{-1.18}$% in our fly ash samples, we estimated a FOC_{ash} flux of $0.21^{+0.15}/_{-0.11}$ and a $f_{FOC\text{-}ash}$ of $37^{+40}/_{-19}$% of the CJ FOC export. In this case, 21% of the unutilized fly ash in the CJ basin enters the rivers (Fig. 4*A*).

Third, we noticed that the FOC content (0.45 ± 0.10%) in our sediment samples from the lower reach of CJ was typically higher than in the samples (0.10 to 0.20%) from regions upstream of the Three Gorges Dam and areas of intense coal consumption (39, 67). Attributing this downstream increase in FOC content to ash input resulted in estimates of $f_{FOC\text{-}ash}$ of ~60 to 80%—values similar to those achieved via mass balance. To formally demonstrate that FOC content increases downstream as a result of fly ash input, one would need more depth-profile sampling to capture variations in riverine OC across hydraulic gradients, and additional accounting for the bedrock and landscape heterogeneities within the CJ basin (e.g., variations in lithology and contributions from different tributaries) (11, 38, 39, 67). Nonetheless, this first-order estimate was similar to that achieved with our two other approaches for quantifying $f_{FOC\text{-}ash}$.

The estimate of $f_{FOC\text{-}ash}$ from the change in MS ($37^{+40}/_{-19}$%) is somewhat lower than the estimate from mass balance calculations ($72^{+8}/_{-12}$%) and the downstream trends in FOC content (~60 to 80%). This discrepancy can be explained because the mass balance calculations assume FOC_{ash} is the only anthropogenic FOC input to the CJ FOC pool. As there may be other anthropogenic sources of fossil carbon, e.g., from petrochemicals (68–70), our

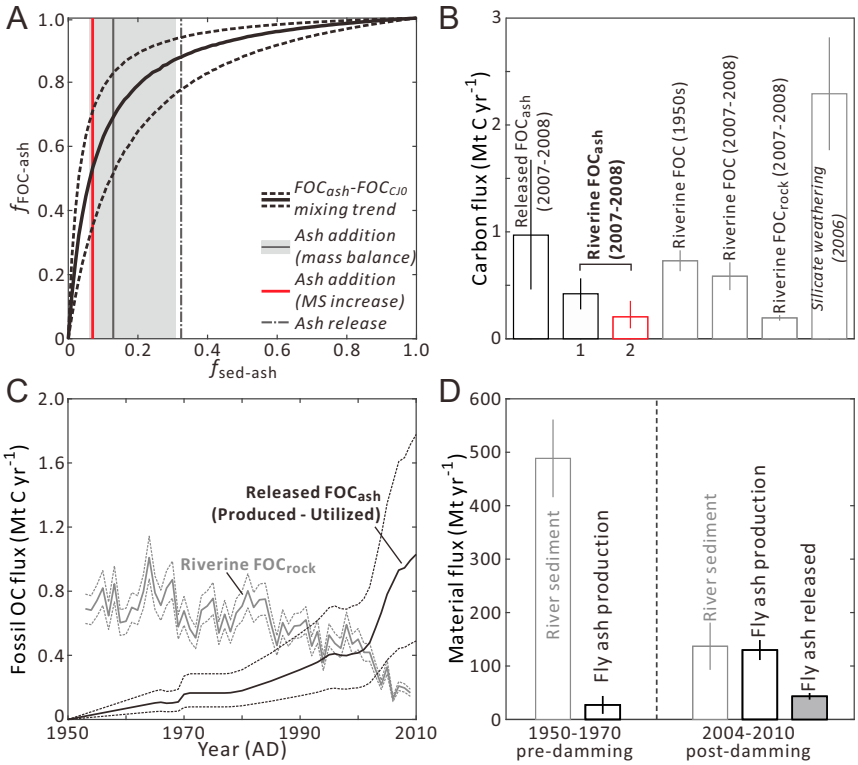

Fig. 4. Fluxes of FOC, fly ash, and sediment in the CJ basin. (*A*) $f_{FOC\text{-}ash}$ (fraction of fly ash-sourced fossil OC in the total flux of fossil OC exported by CJ) as a function of $f_{sed\text{-}ash}$ (mass fraction of fly ash in the total sediment flux) (curves with uncertainty bands determined from Monte Carlo simulations; *SI Appendix*), with the mixing trend between FOC_{ash} and FOC_{CJ0} (FOC in ash-free sediment), fly-ash release (dashed line, difference between produced and utilized fly ash), and estimates of $f_{sed\text{-}ash}$ (red line from changes in MS of the CJ sediment, and black line and gray range from mass balance calculations). (*B*) Different types of carbon flux in the CJ basin where "1" and "2" denote riverine FOC_{ash} flux estimated from mass balance calculations and from changes in MS of CJ sediment, respectively. The released FOC_{ash} flux is estimated from this study as the product of the released fly ash flux and the FOC_{ash} content. The 2007 to 2008 riverine FOC flux is estimated in ref. 35, and the silicate weathering flux (2006) is from ref. 25. The riverine FOC_{rock} flux (2007 to 2008) and the riverine FOC flux (1950s) are quantified from this study. (*C*) Changes of riverine FOC_{rock} flux versus released (produced − utilized) FOC_{ash} flux in 1950 to 2010. (*D*) Sediment flux and fly-ash flux in the CJ basin in 1950 to 1970 (predamming) and 2004 to 2010 (postdamming).

estimate based from mass balance likely sets an upper bound on $f_{FOC\text{-}ash}$ and FOC_{ash} flux.

Overall, the multiple approaches yield results of a similar magnitude, suggesting this estimate of FOC_{ash} flux is robust to a first order. Combining the results above, we concluded that in 2007 to 2008, fly ash contributed a FOC_{ash} flux of 0.21 to 0.42 Mt C·y^{-1}, making up 37 to 72% of the CJ-exported FOC (Fig. 4*B*). For comparison, the estimated atmospheric carbon drawdown via silicate weathering in the basin is 2.29 ± 0.53 Mt C·y^{-1} (Fig. 4*B*) (32).

Fossil Carbon Flux Perturbed by Human Activities. Globally, the total fly ash production during the 2000s was around 750 Mt·y^{-1} (28, 71), with annual global river sediment export estimated at 17,800 Mt·y^{-1} (72). Thus, while the mass flux of fly ash in the CJ now matches the scale of natural sediment transfer in this basin (Fig. 2), the same is not true globally. The globally averaged utilization rate of fly ash is not well determined, but the major coal consumers (China, United States, and India, accounting for 70% of the total consumption) reported an average utilization rate of ∼50% during 2007 to 2008 (28), leaving ∼375 Mt·y^{-1} of fly ash that was not utilized. A global-average FOC_{ash} content is challenging to estimate accurately, because FOC_{ash} depends on a range of factors including coal types and combustion conditions (see expanded discussion in *SI Appendix*, section S6) (23, 24, 45, 51)—conditions that likely vary from region to region. For a first-order constraint, we compiled data on FOC_{ash} content for 247 samples from different regions and found an FOC_{ash} content of $4.70^{+9.69}/_{-3.40}$% (median and 16th to 84th percentiles; *SI Appendix*, section S7 and Fig. S6), which was on the same order of magnitude as the FOC_{ash} content ($2.25^{+1.63}/_{-1.18}$%) measured in our CJ fly-ash samples. Note that most global ash FOC content data were estimated via the loss on ignition—a method that can overestimate the true FOC content and thus may partially explain why the CJ FOC_{ash} content is lower than estimated globally (see more discussion in *SI Appendix*, section S7). Considering the global data compilation, the CJ FOC_{ash} content likely represents a conservative estimate of the actual carbon content in fly ash. Notably, FOC_{ash} contents we measured in CJ ash samples and those from the compiled global dataset were similar to the industrial standards of FOC_{ash} content of 5 to 10% in different countries and regions (*SI Appendix*, section S6) (23, 24, 26, 27); this lent confidence to the overall estimates of the FOC_{ash} flux. If $[FOC]_{ash}$ found in the CJ samples is typical, a global FOC_{ash} yield of $8.43^{+6.11}/_{-4.43}$ Mt C·y^{-1} can be expected. Assuming 20% of the unutilized fly ash is transported by rivers (we found that this number was 13 to 27% for the CJ basin), the global riverine FOC_{ash} flux to the oceans is then $1.69^{+1.22}/_{-0.89}$ Mt C·y^{-1}, making up $3.9^{+12}/_{-3.2}$% of the modern-day riverine FOC flux ($43^{+61}/_{-25}$ Mt C·y^{-1}) (44). Note that this estimate of global FOC_{ash} flux carries large uncertainties, and further studies of FOC_{ash} contents and ash supply to rivers in different regions will be required to improve upon it. Nonetheless, our first-order estimate of the global-average $f_{FOC\text{-}ash}$ of ∼4% is lower than the CJ case (37 to 72%), meaning that the CJ basin likely represents an upper end member in the distribution of FOC_{ash} production and export. So why does the CJ basin have such a high $f_{FOC\text{-}ash}$, and such a dominant overall flux of fly ash? We attributed this to two of the major anthropogenic modifications of the CJ basin: increasing coal consumption and dam construction.

First, coal consumption in China has substantially increased over the past 60 y, boosting fly ash production (Figs. 2 and 4*C*). Hosting China's most economically developed and populated areas, the CJ basin has witnessed intense construction of coal-fired power and steel plants (Fig. 1*C*), providing a major source of FOC_{ash}, especially in its middle and lower reaches (35, 70, 73). In the 2000s, China's consumption increased to more than 50% of the global coal consumption. Alone, all the provinces in the CJ basin comprise 36% of China's coal consumption—a value equivalent to 18% of the global coal consumption. Thus, the CJ basin represents a major locus of fly ash production.

Second, the continued construction of dams and reservoirs in the CJ basin has decreased fluxes of sediment and FOC_{rock}. After the impoundment of the Three Gorges Reservoir in 2003, the CJ sediment export has reduced to ∼100

$Mt{\cdot}y^{-1}$ from ~500 $Mt{\cdot}y^{-1}$ before the dams were emplaced (Fig. 4 *C* and *D*) (34), contributing <1% to the global riverine sediment flux to the oceans (72). Since FOC_{rock} is mainly eroded from upstream areas and scales with sediment flux (38, 44), a significant proportion of FOC_{rock} is being sequestered in the reservoirs, leading to a reduction in the riverine-carried FOC_{rock} flux in the lower CJ reach where many large-scale power and steel plants, the major sources of FOC_{ash}, are located (Fig. 1*C*).

Transport and Fate of Fossil OC. Our analysis revealed that FOC_{ash} and FOC_{rock} have systematically distinct reactivities. When compared overall to biospheric carbon, the low f_{ox} and high E_a values we observed indicated that FOC_{ash} is expected to be significantly more recalcitrant and conserved during transport and storage compared to FOC_{rock}. These differences will affect their fates during fluvial transport and storage, leading to different impacts on the carbon cycle. For FOC_{ash}, the graphitic component is less reactive and is expected to be more conserved as it transits the landscape, whereas the nongraphitic carbon is more reactive and thus more likely to interact with active carbon-cycle processes in surface and subsurface environments (5, 47).

The fate of FOC_{rock} as it becomes exposed to surface processes depends on its chemical properties and the geomorphic setting. We saw that FOC_{rock} in the CJ basin contains a large fraction that is labile and prone to oxidation (Fig. 3), whereas FOC in river sediments is comparatively recalcitrant (38). This suggested the preferential loss of the labile component in FOC_{rock} during denudation, fluvial transport, and sediment storage in the CJ system—a pattern consistent with prior observations of significant oxidation of FOC_{rock} in large floodplain systems (e.g., Amazon) (59). Although laboratory experiments have intimated slow reaction kinetics of FOC_{rock} oxidation (e.g., first-order kinetic coefficients on the order of 10^{-3} to 10^{-4} y^{-1}) (74), the long transit time of OC and sediment (e.g., ~10^4 to 10^5 y) in large floodplain systems (75, 76) matches or exceeds the characteristic reaction timescales of FOC_{rock} and thus would allow sufficient reaction time for FOC_{rock} oxidation. In contrast, FOC_{rock} oxidation might be kinetically limited in river systems with smaller catchment sizes and shorter transit timescales such as the rivers in mountainous islands (8). Overall, we hypothesized that the differences in the reactivity of FOC_{rock} and FOC_{ash} translate into the differences in their fates most profoundly in large alluvial systems (e.g., CJ and Amazon) with long transit times, and such differences are expected to be dampened in smaller catchments with shorter transit times.

Dam building in the CJ basin has probably influenced the fate of FOC_{rock} during fluvial transit as well. Previous studies suggested that the high sedimentation rate in the reservoirs would limit oxygen exposure time of carbon-bearing particles and promote their preservation (11, 38, 39, 64). Thus, the reservoirs in the CJ basin might be expected to help sequester and preserve FOC_{rock} from upstream CJ, buffering its oxidation in downstream floodplains and estuaries (38). In addition, although there has been an increased supply of FOC from coal ash in the middle-lower CJ basin; one prior study hypothesized that the emplacement of the Three Gorges Dam in 2003 would lead to younger and fresher OC exported by the CJ (39). We do not have upstream samples during our study time interval to delineate the downstream changes of riverine OC in 2007 to 2008. However, we noticed that the average proportion of FOC in our 2007 to 2008 sediment samples (~25%) was higher than the FOC proportion in the middle-to-lower CJ sediment samples (~10%) collected 1 to 2 y later after our sampling time. This difference suggested a temporal shift toward a lower proportion of FOC in the CJ-exported OC—a trend consistent with the proposed change toward a younger and fresher riverine OC flux after the impoundment of the Three Gorges Reservoir. Nonetheless, continued monitoring and systematic sampling of the whole CJ fluvial network are needed for a more detailed picture of how hydraulic engineering impacts carbon cycling in this system (38, 39).

FOC_{ash} and FOC_{rock} are also carried by particles of different sizes, which can affect their fate via transport processes. FOC_{ash} is mostly encapsulated in micrometer-sized fly-ash particles, whereas FOC_{rock} is bound to coarser (e.g., sand-sized) grains. Thus, FOC_{ash} could more easily bypass dams during flow release, whereas FOC_{rock} is likely to be sequestered in reservoirs. When delivered to the CJ estuary and the East China Sea margin where hydraulic conditions and sediment transport and storage processes are complex, the fine-grain-carried FOC_{ash} may have more dynamic behavior (e.g., flocculation settling, suspension, and dispersion) and may be spread over a larger depositional area than FOC_{rock} (77). The fine particle sizes that carry FOC_{ash} can also be more efficiently transported by aeolian processes, which can deliver FOC_{ash} to remote areas beyond riverine transport within a given catchment (78). The aeolian flux of FOC_{ash} both within and outside of the CJ basin requires further assessment, but we anticipated that these fluxes are minor compared to the riverine flux, considering the dominance of the wet, monsoonal climate in the basin that limits ash transport by aeolian processes (79, 80). In northern China where a drier climate dominates, aeolian processes may well play a more important role transporting FOC_{ash} (80, 81).

Conclusions and Implications

The CJ basin illustrates how human activities have significantly altered the carbon cycle at continental scales. In the CJ basin, fly ash contributes a remarkable 37 to 72% of the riverine fossil OC exported to the oceans. Driven by the human pursuit of energy, the riverine-carried FOC_{ash} flux has increased while the riverine FOC_{rock} flux decreased—and as a result, these two fluxes have converged over an interval of 60 y to amplify the concentration of FOC_{ash} on the landscape. This serves as an example of how the pace of the human-induced alteration of the carbon cycle can catch up with nature-sourced carbon at decadal timescales and demarcates another dimension of the human imprint on the short-term carbon cycle beyond that directly associated with CO_2 emission during fossil fuel combustion (19, 82).

Our results showed that not all fossil OC is made equal: FOC_{rock} has a significant fraction that is labile and can be oxidized during transport, whereas FOC_{ash} is highly recalcitrant (i.e., unreactive) and can be conserved during transport. While coal burning is a leaky process with respect to OC, the way that carbon is transformed by incomplete combustion means that the FOC_{ash} that escapes this process is much less likely to end up as CO_2 compared to the FOC_{rock} naturally derived from erosion. Furthermore, its fossil origin means FOC_{ash} is radiocarbon-dead (7, 11). With increasing coal consumption and ash production (19), FOC_{ash} flux is expected to increase and to contribute to a greater proportion of the total riverine FOC flux to the oceans. With this growing human-induced carbon flux, caution will need to be taken when interpreting radiocarbon-based material flux as well as records from recent offshore sediments. With this observation in mind, given that the magnitude of fly ash release can match natural sediment fluxes at regional scales (e.g., in the CJ basin), the unique properties of FOC_{ash} make it a useful tracer of anthropogenic impacts on the OC cycle. By reflecting the history of coal consumption, FOC_{ash} in sedimentary cores and other archives could provide a distinct marker of the Anthropocene (78, 83).

Data Availability. All study data are included in the article and/or supporting information.

ACKNOWLEDGMENTS. This project was funded by the National Key R&D Program of China (Grant 2017YFD0800300). G.K.L. acknowledges support from a California Institute of Technology Geology Option Postdoctoral Fellowship and a National Ocean Sciences Accelerator Mass Spectrometry Laboratory Graduate Intern Fellowship. W.W.F. and M.P.L. acknowledge support from Foster and Coco Stanback, California Institute of Technology's Terrestrial Hazard Observation and Reporting Center, and the Resnick Sustainability Institute. We thank Yuliang Chen for help with data compilation.

1. R. A. Berner, A. C. Lasaga, R. M. Garrels, The carbonate-silicate geochemical cycle and its effect on atmospheric carbon dioxide over the past 100 million years. *Am. J. Sci.* **283**, 641–683 (1983).
2. R. A. Berner, The long-term carbon cycle, fossil fuels and atmospheric composition. *Nature* **426**, 323–326 (2003).
3. R. A. Berner, Atmospheric carbon dioxide levels over phanerozoic time. *Science* **249**, 1382–1386 (1990).
4. L. A. Derry, C. France-Lanord, Neogene growth of the sedimentary organic carbon reservoir. *Paleoceanography* **11**, 267–275 (1996).
5. V. Galy, O. Beyssac, C. France-Lanord, T. Eglinton, Recycling of graphite during Himalayan erosion: A geological stabilization of carbon in the crust. *Science* **322**, 943–945 (2008).
6. E. T. Sundquist, K. Visser, "The geologic history of the carbon cycle" in *Treatise on Geochemistry*, H. D. Holland, K. K. Turekian, Eds. (Elsevier, 2014), vol. 10, pp. 361–398.
7. N. E. Blair, The persistence of memory: The fate of ancient sedimentary organic carbon in a modern sedimentary system. *Geochim. Cosmochim. Acta* **67**, 63–73 (2003).
8. R. G. Hilton, A. Galy, N. Hovius, M. J. Horng, H. Chen, Efficient transport of fossil organic carbon to the ocean by steep mountain rivers: An orogenic carbon sequestration mechanism. *Geology* **39**, 71–74 (2011).

9. J. D. Hemingway *et al*., Microbial oxidation of lithospheric organic carbon in rapidly eroding tropical mountain soils. *Science* **360**, 209–212 (2018).
10. K. Horan *et al*., Mountain glaciation drives rapid oxidation of rock-bound organic carbon. *Sci. Adv.* **3**, e1701107 (2017).
11. V. Galy *et al*., Efficient organic carbon burial in the Bengal fan sustained by the Himalayan erosional system. *Nature* **450**, 407–410 (2007).
12. G. Shrestha, S. Traina, C. Swanston, Black carbon's properties and role in the environment: A comprehensive review. *Sustainability* **2**, 294–320 (2010).
13. T. C. Bond *et al*., Bounding the role of black carbon in the climate system: A scientific assessment. *J. Geophys. Res. D Atmos.* **118**, 5380–5552 (2013).
14. A. I. Coppola *et al*., Global-scale evidence for the refractory nature of riverine black carbon. *Nat. Geosci.* **11**, 584–588 (2018).
15. C. A. Masiello, E. R. M. Druffel, Black carbon in deep-sea sediments. *Science* **280**, 1911–1913 (1998).
16. X. Wang, C. Xu, E. M. Druffel, Y. Xue, Y. Qi, Two black carbon pools transported by the Changjiang and Huanghe Rivers in China. *Global Biogeochem. Cycles* **30**, 1778–1790 (2016).
17. A. I. Coppola *et al*., Marked isotopic variability within and between the Amazon River and marine dissolved black carbon pools. *Nat. Commun.* **10**, 4018 (2019).
18. M. W. Jones, C. Santín, G. R. van der Werf, S. H. Doerr, Global fire emissions buffered by the production of pyrogenic carbon. *Nat. Geosci.* **12**, 742–747 (2019).
19. IPCC, *Climate change 2013: The Physical Science Basis. Contribution of Working Group I to the Fifth Assessment Report of the Intergovernmental Panel on Climate Change* (Cambridge University Press, Cambridge, UK, 2013).
20. BP, "BP Statistical Review of World Energy 2019" (BP, 2019).
21. J. P. Baltrus, A. W. Wells, D. J. Fauth, J. R. Diehl, C. M. White, Characterization of carbon concentrates from coal-combustion fly ash. *Energy Fuels* **15**, 455–462 (2001).
22. L. Bartoňová, Unburned carbon from coal combustion ash: An overview. *Fuel Process. Technol.* **134**, 136–158 (2015).
23. J. C. Hower *et al*., Coal-derived unburned carbons in fly ash: A review. *Int. J. Coal Geol.* **179**, 11–27 (2017).
24. Y. Xing *et al*., Separation of unburned carbon from coal fly ash: A review. *Powder Technol.* **353**, 372–384 (2019).
25. M. Ahmaruzzaman, A review on the utilization of fly ash. *Pror. Energy Combust. Sci.* **36**, 327–363 (2010).
26. N. S. Dong, *Reducing Carbon-in-Ash* (IEA Clean Coal Centre, 2010).
27. ASTM International, "ASTM C618-15: Standard specification for coal fly ash and raw or calcined natural pozzolan for use in concrete" (ASTM International, West Conshohocken, PA, 2015).
28. Z. T. Yao *et al*., A comprehensive review on the applications of coal fly ash. *Earth Sci. Rev.* **141**, 105–121 (2015).
29. National Bureau of Statistics of China, *China Statistical Yearbook* (National Bureau of Statistics of China, 2009).
30. Z. Chen, J. Li, H. Shen, W. Zhanghua, Yangtze River of China: Historical analysis of discharge variability and sediment flux. *Geomorphology* **41**, 77–91 (2001).
31. J. S. Chen, F. Y. Wang, X. H. Xia, L. T. Zhang, Major element chemistry of the Changjiang (Yangtze River). *Chem. Geol.* **187**, 231–255 (2002).
32. B. Chetelat *et al*., Geochemistry of the dissolved load of the Changjiang Basin rivers: Anthropogenic impacts and chemical weathering. *Geochim. Cosmochim. Acta* **72**, 4254–4277 (2008).
33. J. Hartmann, N. Moosdorf, The new global lithological map database GLiM: A representation of rock properties at the Earth surface. *Geochem. Geophys. Geosyst.* **13**, Q12004 (2012).
34. X. Q. Chen, Y. X. Yan, R. S. Fu, X. P. Dou, E. F. Zhang, Sediment transport from the Yangtze River, China, into the sea over the post-three Gorge dam period: A discussion. *Quat. Int.* **186**, 55–64 (2008).
35. D. Tong *et al*., Targeted emission reductions from global super-polluting power plant units. *Nat. Sustain.* **1**, 59–68 (2018).
36. S. L. Yang, J. Zhang, X. J. Xu, Influence of the Three Gorges Dam on downstream delivery of sediment and its environmental implications, Yangtze River. *Geophys. Res. Lett.* **34**, L10401 (2007).
37. S. L. Yang *et al*., Impact of dams on Yangtze River sediment supply to the sea and delta intertidal wetland response. *J Geophys Res-Earth* **110**, F03006 (2005).
38. G. Li *et al*., Dam-triggered organic carbon sequestration makes the Changjiang (Yangtze) River basin (China) a significant carbon sink. *J. Geophys. Res. Biogeosci.* **120**, 39–53 (2015).
39. Y. Wu, T. I. Eglinton, J. Zhang, D. B. Montlucon, Spatiotemporal variation of the quality, origin, and age of particulate organic matter transported by the Yangtze River (Changjiang). *J. Geophys. Res. Biogeosci.* **123**, 2908–2921 (2018).
40. F. L. Li, G. J. Li, J. F. Ji, Increasing magnetic susceptibility of the suspended particles in Yangtze River and possible contribution of fly ash. *Catena* **87**, 141–146 (2011).
41. X. Wang, A. Li, Preservation of black carbon in the shelf sediments of the East China Sea. *Chin. Sci. Bull.* **52**, 3155–3161 (2007).
42. Z.-H. Wang *et al*., Dating recent sediments from the subaqueous Yangtze Delta and adjacent continental shelf, China. *J. Palaeogeogr.* **3**, 207–218 (2014).
43. N. L. Rose *et al*., Sedimentary evidence for changes in the pollution status of Taihu in the Jiangsu region of eastern China. *J. Paleolimnol.* **32**, 41–51 (2004).
44. V. Galy, B. Peucker-Ehrenbrink, T. Eglinton, Global carbon export from the terrestrial biosphere controlled by erosion. *Nature* **521**, 204–207 (2015).
45. C. Heidrich, H.-J. Feuerborn, A. Weir, Coal combustion products: A global perspective. *VGB Power Tech* **93**, 46–52 (2013).
46. B. G. Kutchko, A. G. Kim, Fly ash characterization by SEM–EDS. *Fuel* **85**, 2537–2544 (2006).
47. M. Li *et al*., Role of elemental carbon in the photochemical aging of soot. *Proc. Natl. Acad. Sci. U.S.A.* **115**, 7717–7722 (2018).
48. U. G. Surabhi, N. Suresh, Characterization of unburnt carbon recovered from fly ash by froth flotation. https://www.semanticscholar.org/paper/Characterization-of-Unburnt-Carbon-Recovered-from-Surabhi-Udayabhanu/40b8214b4b05d64dde12139914353f1ec8b839c4. Accessed 23 April 2021.
49. Y.-M. Gao, H.-S. Shim, R. H. Hurt, E. M. Suuberg, N. Y. C. Yang, Effects of carbon on air entrainment in fly ash concrete: The role of soot and carbon black. *Energy Fuels* **11**, 457–462 (1997).
50. J. C. Hower, U. M. Graham, A. Dozier, M. T. Tseng, R. A. Khatri, Association of the sites of heavy metals with nanoscale carbon in a Kentucky electrostatic precipitator fly ash. *Environ. Sci. Technol.* **42**, 8471–8477 (2008).
51. S. R. Dindarloo, J. C. Hower, Prediction of the unburned carbon content of fly ash in coal-fired power plants. *Coal Combust. Gasif. Prod.* **7**, 19–29 (2015).
52. Z. Hao, X. Qian, K. Cen, F. Jianren, Optimizing pulverized coal combustion performance based on ANN and GA. *Fuel Process. Technol.* **85**, 113–124 (2004).
53. J. M. Veranth, T. H. Fletcher, D. W. Pershing, A. F. Sarofim, Measurement of soot and char in pulverized coal fly ash. *Fuel* **79**, 1067–1075 (2000).
54. R. Sparkes, N. Hovius, A. Galy, R. V. Kumar, J. T. Liu, Automated analysis of carbon in powdered geological and environmental samples by Raman spectroscopy. *Appl. Spectrosc.* **67**, 779–788 (2013).
55. M. Al-Hajeri *et al*., Maturity estimation for Type II-S kerogen using Raman spectroscopy – A case study from the Najmah and Makhul Formations in Kuwait. *Int. J. Coal Geol.* **217**, 103317 (2020).
56. J. D. Hemingway, D. H. Rothman, S. Z. Rosengard, V. V. Galy, Technical note: An inverse method to relate organic carbon reactivity to isotope composition from serial oxidation. *Biogeosciences* **14**, 5099–5114 (2017).
57. K. C. Huang, R. A. Couttenye, G. E. Hoag, Kinetics of heat-assisted persulfate oxidation of methyl tert-butyl ether (MTBE). *Chemosphere* **49**, 413–420 (2002).
58. M. Helfrich, H. Flessa, R. Mikutta, A. Dreves, B. Ludwig, Comparison of chemical fractionation methods for isolating stable soil organic carbon pools. *Eur. J. Soil Sci.* **58**, 1316–1329 (2007).
59. J. Bouchez *et al*., Oxidation of petrogenic organic carbon in the Amazon floodplain as a source of atmospheric CO_2. *Geology* **38**, 255–258 (2010).
60. R. G. Hilton, J. Ó. Gaillardet, D. Calmels, J. L. Birck, Geological respiration of a mountain belt revealed by the trace element rhenium. *Earth Planet. Sci. Lett.* **403**, 27–36 (2014).
61. O. R. Harvey *et al*., An index-based approach to assessing recalcitrance and soil carbon sequestration potential of engineered black carbons (biochars). *Environ. Sci. Technol.* **46**, 1415–1421 (2012).
62. J. I. Hedges, R. G. Keil, Sedimentary organic matter preservation: An assessment and speculative synthesis. *Mar. Chem.* **49**, 81–115 (1995).
63. J. D. Hemingway *et al*., Mineral protection regulates long-term global preservation of natural organic carbon. *Nature* **570**, 228–231 (2019).
64. N. E. Blair, R. C. Aller, The fate of terrestrial organic carbon in the marine environment. *Annu. Rev. Mar. Sci.* **4**, 401–423 (2012).
65. S. Y. Yang *et al*., Burial of organic carbon in Holocene sediments of the Zhujiang (Pearl River) and Changjiang (Yangtze River) estuaries. *Mar. Chem.* **123**, 1–10 (2011).
66. Chang Jiang Water Commission, "Chang Jiang sediment bulletin" (Chang Jiang Water Commission, 2009).
67. J. Wang, The isotopic composition and fluxes of particulate organic carbon exported from the eastern margin of the Tibetan Plateau. *Geochim. Cosmochim. Acta* **252**, 1–15 (2019).
68. J. Liggio *et al*., Are emissions of black carbon from gasoline vehicles underestimated? Insights from near and on-road measurements. *Environ. Sci. Technol.* **46**, 4819–4828 (2012).
69. A. Mah, X. Wang, Accumulated injuries of environmental injustice: Living and working with petrochemical pollution in Nanjing, China. *Ann. Assoc. Am. Geogr.* **109**, 1961–1977 (2019).
70. Y. Liu *et al*., Distribution and sources of polycyclic aromatic hydrocarbons in surface sediments of rivers and an estuary in Shanghai, China. *Environ. Pollut.* **154**, 298–305 (2008).
71. National Development and Reform Commission of China, Annual report on comprehensive utilization of resources of China. http://www.gov.cn/gzdt/2013-04/08/content_2372577.htm [in Chinese]. Accessed 19 April 2021.
72. J. P. M. Syvitski, C. J. Vörösmarty, A. J. Kettner, P. Green, Impact of humans on the flux of terrestrial sediment to the global coastal ocean. *Science* **308**, 376–380 (2005).
73. F. Liu *et al*., High-resolution inventory of technologies, activities, and emissions of coal-fired power plants in China from 1990 to 2010. *Atmos. Chem. Phys.* **15**, 13299–13317 (2015).
74. S. Chang, R. A. Berner, Coal weathering and the geochemical carbon cycle. *Geochim. Cosmochim. Acta* **63**, 3301–3310 (1999).
75. M. Repasch *et al*., Sediment transit time and floodplain storage dynamics in alluvial rivers revealed by meteoric 10Be. *J. Geophys. Res. Earth Surf.* **125**, e2019JF005419 (2020).

76. A. Dosseto, B. Bourdon, S. P. Turner, Uranium-series isotopes in river materials: Insights into the timescales of erosion and sediment transport. *Earth Planet. Sci. Lett.* **265**, 1–17 (2008).
77. M. P. Lamb *et al*., Mud in rivers transported as flocculated and suspended bed material. *Nat. Geosci.* **13**, 566–570 (2020).
78. J. R. McConnell *et al*., 20th-century industrial black carbon emissions altered Arctic climate forcing. *Science* **317**, 1381–1384 (2007).
79. K. Pye, The nature, origin and accumulation of loess. *Quat. Sci. Rev.* **14**, 653–667 (1995).
80. H. Song, K. Zhang, S. Piao, S. Wan, Spatial and temporal variations of spring dust emissions in northern China over the last 30 years. *Atmos. Environ.* **126**, 117–127 (2016).
81. G. Li, J. Chen, J. Ji, J. Yang, T. M. Conway, Natural and anthropogenic sources of East Asian dust. *Geology* **37**, 727–730 (2009).
82. R. A. Houghton, "10.10 - the contemporary carbon cycle" in *Treatise on Geochemistry*, H. D. Holland, K. K. Turekian, Eds. (Elsevier, Oxford, ed. 2, 2014), pp. 399–435.
83. N. L. Rose, Spheroidal carbonaceous fly ash particles provide a globally synchronous stratigraphic marker for the Anthropocene. *Environ. Sci. Technol.* **49**, 4155–4162 (2015).